JOURNAL OF MATERIALS SCIENCE 32 (1997) 589–601

Thermal stability of transition phases in zirconia-doped alumina

B. DJURIČIĆ*, S. PICKERING, P. GLAUDE, D. MCGARRY, P. TAMBUYSER
Institute for Advanced Materials, Joint Research Centre, 1755 ZG Petten, Netherlands

Alumina was prepared from an aqueous salt solution by homogeneous precipitation followed by calcination in air. Dependence of the thermal stability of transition phases on the presence of a zirconia dopant and on autoclave treatment prior to calcination was investigated using X-ray diffraction (XRD), differential thermal analysis coupled with thermogravimetric analysis (DTA–TGA) and transmission electron microscope (TEM) analysis. Homogeneous precipitation produced an amorphous trihydrate precipitate; the autoclave treatment converted this to crystalline boehmite (monohydrate). The zirconia was soluble in the transition alumina but was insoluble in α-Al_2O_3 so that phase transformation to α-Al_2O_3 was accompanied by a phase separation to form an alumina-zirconia nanocomposite. The thermal stability of the transition phases was increased both by the dopant and by the autoclave treatment. A combination of both parameters yielded the most stable transition alumina, which withstood 1 h at 1200 °C without transformation to α-Al_2O_3.

1. Introduction

Gamma alumina and its related transition forms have well established applications in separation technologies that require nanoscale porosity, and in catalysis where high specific surface area and catalytically active surface sites are needed. In these applications, the ability of transition aluminas to maintain their properties at elevated temperatures is of decisive importance. However, transition aluminas are metastable phases, and at about 1000 °C there is a transformation to α-Al_2O_3 with a catastrophic loss of specific surface area and a change in surface chemistry, which destroys their usefulness in both applications. There is, therefore, considerable interest in improving the thermal stability of transition phase aluminas so that processes can be operated at higher temperatures with a corresponding gain in efficiency. Stabilization of the metastable phases depends on inhibiting nucleation of α-Al_2O_3. Nucleation cannot occur as long as the primary particle size of the transition aluminas is smaller than the critical nucleus size for the α-Al_2O_3. However, even if the primary particle size does grow to exceed the critical nucleus size, then the nucleation of α-Al_2O_3 will still depend on the availability of suitable nucleation sites. Thermal stability therefore depends both on particle morphology and on features in the crystal structure, particularly at surfaces, that can act as nucleation sites. If we wish to optimize thermal stability, we need both to inhibit processes that lead to particle growth, such as sintering, and to deactivate potential nucleation sites. Structural stability can only be improved through structural modification. In practice, the structural morphology of transition aluminas, and hence their thermal stability, can be modified either through the choice of appropriate synthesis conditions, or by the use of cationic dopants.

Transition aluminas are prepared by the dehydration of certain alumina hydrates, i.e. boehmite (AlOOH), gibbsite [$Al(OH)_3$], and bayerite [$Al(OH)_3$]. However, one other hydrate, diaspore (AlOOH), transforms directly to α-Al_2O_3 at about 500 °C, apparently because the oxygen ions in diaspore are hexagonally close packed (h.c.p.) as in α-Al_2O_3. In contrast, the distribution of the oxygen ions in boehmite, gibbsite and bayerite is closer to cubic close packing (c.c.p.), and their thermal transformation follows a typical sequence, for example

$$\text{boehmite} \rightarrow \gamma \rightarrow \delta \rightarrow \theta \rightarrow \alpha\text{-}Al_2O_3$$

The specific transformation sequence and the transformation temperatures depend on the structure of the hydrate precursor. The crystal structures of the transition aluminas are γ (cubic spinel), δ (orthorhombic), θ (monoclinic) but they all share the same c.c.p. oxygen sublattice and differ in the distribution of the aluminium cations between the octahedral and tetrahedral sites. Consequently, a characteristic feature of these transformations is that the basic pattern of atomic arrangement appears to change very little during the transformation sequence until the final transition to α-Al_2O_3, which involves a major structural rearrangement. The structure of the transition aluminas therefore can be rather complex [1–8] reflecting characteristics inherited from the hydrated

*Current affiliation: Koninklijke Hoogovens, Research & Development, Postbus 10000, 1970 CA IJmuiden, Netherlands.

0022–2461

alumina, which in turn depend on the precipitation conditions. The properties that are relevant to catalysis and membrane applications, such as pore size and pore size distribution, therefore depend both on the chemical nature of the precursor and on the details of the synthesis conditions. Conditions such as the hydrothermal treatment of an alkoxide-derived gel [9], spray pyrolysis of a boehmite sol [10], and treatment under supercritical conditions [11] have all been investigated as methods for modifying the structure of transition aluminas to increase their thermal stability.

The most effective dopants for increasing the thermal stability of transition aluminas will be those that reduce particle growth through sintering, and that also neutralize potential α-Al_2O_3 nucleation sites. The rate limiting step in the sintering of transition aluminas is believed to be the dissociative adsorption of water molecules onto an anionic vacancy, thereby allowing migration of the adjacent "AlO" molecular unit [12, 13]. Nucleation of α-Al_2O_3 is believed to occur by an annihilation reaction between cationic and anionic vacancies leading to a restructuring of the oxygen sublattice from c.c.p. to h.c.p. [12, 13]. The anion vacancies are created by the dehydroxylation process and cation vacancies exist due to the intrinsically cation defective nature of the spinel lattice.

Si and La are examples of effective dopants. Si dopant forms Si–O–Si and Si–O–Al bridges on the surface of the transition alumina, which give surface properties similar to those of silica [14]. These bridges act to remove anionic vacancies from the alumina surface [15], thereby impeding the mechanisms for sintering and α-Al_2O_3 nucleation. Lanthanum is believed to form a low-surface-energy surface layer of lanthanum aluminate ($LaAlO_3$) in which the oxygen sublattice is coherent with that of the underlying transition alumina. Because this layer is effective at less than monolayer concentrations, it is suggested that it forms preferentially at anionic vacancies (Lewis acid sites) that are believed to act as nucleation sites for α-Al_2O_3 as well as being catalytically active sites. Lanthanum aluminate therefore impedes both sintering and the nucleation of α-Al_2O_3 at cation concentrations of about 1%. Other lanthanides behave similarly. At higher additive concentrations and higher temperatures, the lanthanides form β-Al_2O_3 phases in which layers of spinel-like γ-Al_2O_3 are intercalated by La planes. This structure is stable against transformation to α-Al_2O_3 and resists sintering because cation diffusion is difficult perpendicular to the intercalation planes. This phase can therefore maintain a relatively high specific surface area to high temperatures. Many cations, i.e. alkali metals such as barium, also form aluminates and β-Al_2O_3 in an analogous fashion and these may therefore be considered as candidate dopant elements. In particular, Ba has been studied [16, 17] for use as a dopant for alumina to create a high temperature catalyst.

In this work we report on the effects of Zr dopant and processing parameters on the thermal stability of transition aluminas. Zr is of interest as a dopant because it forms extensive solid solutions with transition alumina but is insoluble in α-Al_2O_3. The partition of ZrO_2 from transition Al_2O_3 therefore constitutes a barrier to the transformation to α-Al_2O_3. Autoclave treatment is of interest as it induces a preferential dehydroxylation to form boehmite. Spherical particles of a pure alumina reference powder were synthesized by calcining precipitates made by the forced hydrolysis of aluminium sulfate in the presence of urea. Zr-doped material was made in the same manner, coprecipitating Al and Zr salts to ensure a highly uniform initial distribution. The thermal stability of the transition phases in these two materials was characterized using DTA–TGA, XRD and TEM techniques. The influences of autoclave treatment and of the Zr dopant on the thermal stability of transition alumina were determined both singly and in combination.

2. Experimental procedure

The following starting materials were used in their as-received state: aluminium sulfate octadecahydrate [$(Al_2(SO)_4)_3 \cdot 18H_2O$, chemically pure)] zirconium sulfate tetrahydrate [$(Zr(SO)_4 \cdot 4H_2O)$, 99.99% pure], urea (high purity CON_2H_4) Polyvinylpyrrolidone K-30 (PVP, special grade), nitric acid (reagent grade HNO_3).

An aqueous stock solution was prepared containing 5×10^{-3} mol l^{-1} aluminium sulfate, 1 mol l^{-1} urea and 0.2 wt % PVP. Nitric acid was added to the stock solution until pH 2 was obtained. Spherical particles were precipitated from 31 samples of this solution by heating to 85 °C for 2 h [18, 19]. Various levels of zirconium doping were achieved by adding zirconium sulfate to the solution before precipitation in quantities equivalent to 0.1, 1.0 or 3.0 mol % zirconia. The precipitates were washed with 600 ml water (pH = 9.5) and separated by centrifugation (645 g). This washing procedure was repeated four times. Glass containers were used for all these procedures. The precipitates were then either redispersed in isopropyl alcohol and dried at 95–100 °C in air for 24 h, or were subjected to a hydrothermal treatment. The hydrothermal treatment consisted of heating in an autoclave to about 210 °C for 6 h using a heating rate of about 1 °C min^{-1} to obtain a gel-like product that was then dried in air at 95–100 °C for 24 h. Precipitates were designated either "A" for pure alumina or "AZ" for zirconia-doped alumina. Autoclave treated material received the additional designation "(a)". Consequently, four basic samples designations were used.

A	pure alumina, air-dried	(reference material)
A(a)	pure alumina, autoclave treated	(hydrothermal treatment)
AZ	zirconia-doped alumina, air-dried	(dopant)
AZ(a)	zirconia-doped alumina, autoclave treated	(dopant plus hydrothermal treatment)

Each batch of precipitate was divided into four samples for calcination at 600, 800, 1000 or 1200 °C. The samples were calcined in alumina crucibles for 1 h in a static air atmosphere using a heating rate of

$5\,^{\circ}C\,min^{-1}$. In one case a sample was calcined for 100 h at 1200 °C.

The samples were characterized before calcination using scanning electron microscopy (SEM) (Zeiss DSM 940), DTA and TGA (Netsch STA 409). The DTA–TGA was carried out in air at a heating rate of $5\,^{\circ}C\,min^{-1}$ to 1400 °C. After calcination, the powders were characterized by XRD (Philips PW 173), TEM (Philips EM400) and specific surface area analysis (Brunauer–Emmett–Teller, BET) (Coulter-Omnisorp 360) using nitrogen.

SEM sample preparation for the air-dried precipitates consisted of dispersing the particles in isopropyl alcohol by ultrasonification and then allowing a drop of the suspension to evaporate on the SEM sample holder. For the gel-like product of the autoclave treatment, a small amount of wet gel was placed on the sample holder and dried at 50 °C for 1 h. The samples were coated with carbon before examination. The TEM samples were prepared in a similar way on carbon-coated copper grids.

XRD was used to determine the phases present in the calcined powders and to estimate the apparent crystallite size, D_{app}, from peak broadening using the Scherrer equation, i.e. $D_{app} = K\lambda/(B\cos\theta)$, where $K = 0.9$, λ was the wavelength and B was the peak width obtained using a Voigt peak fitting routine. CuK_α radiation with a graphite filter was used ($\lambda = 0.154\,060$ nm) and instrumental broadening was determined using a LaB_6 standard.

3. Results

The composition of the particles directly after precipitation is reported to be hydrated basic aluminium sulfate with a molar ratio of $[Al^{3+}]/[SO_4^{2-}]$ in the range 2.5–3.5 depending on the precursor salt concentration [18, 19]. However, by washing the precipitate with ammonium hydroxide solution (pH = 9.5) this ratio can be increased to $>100:1$ by an ion-exchange process.

The morphology of the washed particles is shown in Fig. 1 for pure material and for material doped with an amount of Zr equivalent to 1 mol % ZrO_2. The particles of the pure material, Fig. 1a, were monodispersed spheres about 500 nm in diameter, whereas the particles of the Zr-doped material, Fig. 1b, were somewhat smaller and less monodispersed. The latter particles were also linked together into agglomerates by a gel-like substance that may be a precipitate that formed on cooling the solution. Autoclave treatment transformed particles of both the pure and Zr-doped materials into porous gel-like solids as shown in Fig. 2a and b, respectively.

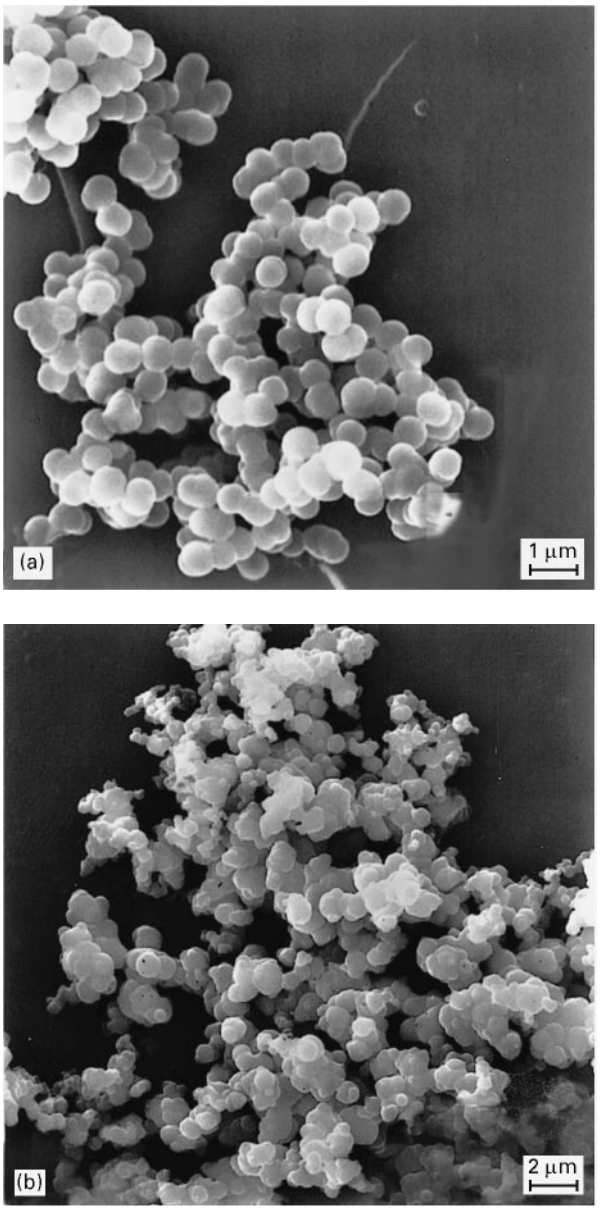

Figure 1 SEM micrographs showing the morphology of precipitate powders dried at 80 °C: (a) undoped material and (b) Zr-doped material.

3.1. XRD analysis

XRD analysis showed that the change from amorphous spherical particles to a gel-like morphology in the autoclaved samples was associated with the crystallization of boehmite. Fig. 3 compares the XRD spectra made after calcination for all materials. The non-autoclaved materials, i.e. samples A and AZ, have very similar XRD spectra and the influence of the Zr dopant was almost undetectable in these spectra. The A and AZ samples remained essentially amorphous up to 800 °C, crystallized to γ-Al_2O_3 at 1000 °C, and to α-Al_2O_3 at 1200 °C. There was just a trace of θ-Al_2O_3 present in the AZ sample at 1200 °C.

In contrast, the presence of Zr dopant in the autoclaved material did produce significant stabilization of the transition alumina. Both the A(a) and AZ(a) samples initially consisted of well crystallized boehmite that transformed to γ-Al_2O_3 at 600 °C. At 1000 °C both samples consisted of a mixture of γ-Al_2O_3 and δ-Al_2O_3 as indicated by a doubling of the 4 0 0 and 4 4 0 peaks. But at 1200 °C the A(a) sample transformed to α-Al_2O_3 and the AZ(a) sample transformed to θ-Al_2O_3. However, it was only the AZ(a) sample doped with 1 mol % ZrO_2 that showed this behaviour, and further ageing at 1200 °C for 100 h transformed the θ-Al_2O_3 to α-Al_2O_3. The AZ(a) samples containing 0.1 and 3.0 mol % ZrO_2 transformed to

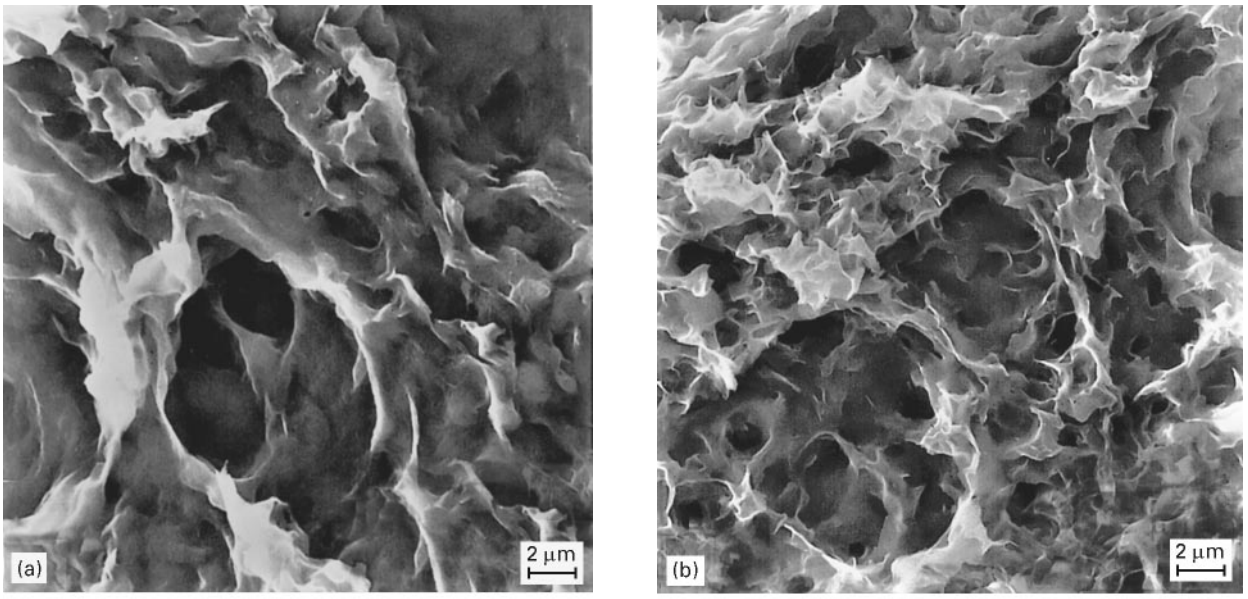

Figure 2 SEM micrographs showing the gel-like morphology of the precipitate autoclaved at 210 °C: (a) undoped material, and (b) Zr-doped material.

α-Al_2O_3 after 1 h at 1200 °C. All subsequent work with Zr-doped material was performed with 1 mol % ZrO_2. Table I summarizes the lattice parameters of the phases present and the average crystallite size and lattice strain. The values are in good agreement with published data [3, 6, 7, 20].

3.2. DTA–TGA analysis

Additional information on the nature of the thermal transformation was provided by DTA–TGA measurements as shown in Fig. 4. The specimens have all already received some thermal treatment, i.e. dried at 95–100 °C or autoclaved at 210 °C, so that events at temperatures lower than these must be attributed to reversible events, i.e. the well defined endothermic peaks at approximately 90–100 °C in autoclaved materials corresponding to the dehydration of less than 1 mole H_2O per mole Al_2O_3.

In the non-autoclaved specimens, i.e. samples A and AZ, there was a progressive loss of weight due to dehydration and dehydroxylation up to about 500 °C without well defined thermal events in a manner characteristic of an amorphous structure. A further weight loss of about 5% occurred between 800–900 °C that seemed to be associated with a small exothermic peak at about 900 °C; this peak may indicate crystallization to γ-Al_2O_3, although Sacks *et al.* [19] attributed a similar exothermic peak at approximately 925 °C to desulfurization. The total weight loss of about 45% was consistent with the loss of 3 moles H_2O per mole Al_2O_3. The formation of α-Al_2O_3 was indicated by an exothermic peak at approximately 1210 °C in sample A and at 1245 °C in sample AZ. This indicates that the Zr-dopant slightly retarded the formation of α-Al_2O_3 and shifted the exothermic crystallization peak by about 35 °C.

In contrast, the autoclaved materials, i.e. samples A(a) and AZ(a), exhibited strong and relatively well defined endothermic DTA peaks at 473–483 °C, and the corresponding non-reversible weight loss of about 15% was attributed to dehydroxylation of boehmite. (The XRD spectra showed that samples A(a) and AZ(a) initially consisted of boehmite.) A further weight loss (8–9%) between 500 and 1000 °C suggested further dehydroxylation and/or removal of anion impurities. This stage of the weight-loss process was more progressive than in the equivalent stage for non-autoclaved materials and no exothermic peak was seen to indicate the formation of γ-Al_2O_3. However, XRD analysis indicated that γ-Al_2O_3 was present and that it formed at a lower temperature than in the non-autoclaved samples. The total weight loss of about 33–35% for the autoclaved materials was significantly less than in the case of samples A and AZ and was consistent with the monohydrate composition of boehmite. The formation of α-Al_2O_3 was clearly visible as an exothermic peak at approximately 1235 °C in sample A(a) and at 1320 °C in the AZ(a) sample. The Zr dopant therefore appears to retard the formation of α-Al_2O_3 rather more than in the non-autoclaved samples. The DTA results therefore suggest that the Zr-dopant and the autoclave treatment both contribute individually to increasing the thermal stability of transition aluminas and that the greatest increase is obtained from these two parameters in combination.

3.3. Specific surface area measurements

The specific surface area (SSA) depended on sample composition and treatment as shown in Fig. 5. The highest SSA ($280\,m^2\,g^{-1}$) was found in the AZ(a) sample after calcination at 600 °C. The difference between the samples became less marked at higher calcination temperatures, but for the samples calcined at 1200 °C sample AZ(a) still had the highest SSA ($36\,m^2\,g^{-1}$) due to the retention of θ-Al_2O_3.

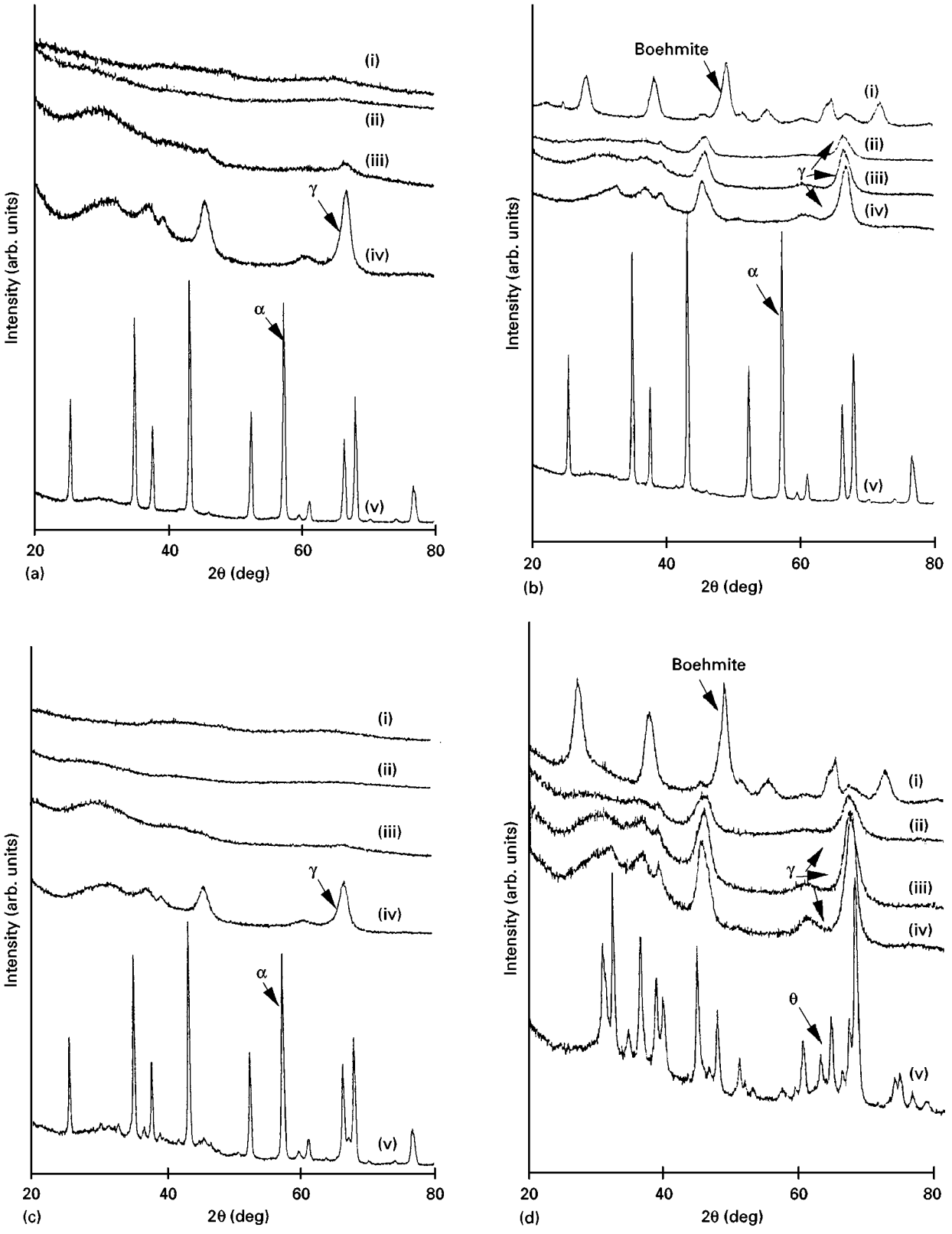

Figure 3 X-ray spectra of various alumina samples after calcination for 1 h at the temperatures, indicated: (a) sample A, (b) sample A(a), (c) sample AZ, (d) sample AZ(a) at (i) 80 °C, (ii) 600 °C, (iii) 800 °C, (iv) 1000 °C, (v) 1200 °C.

3.4. TEM results

In the uncalcined condition, only the boehmite that precipitated in the autoclave treated samples was suitable for TEM examination. The boehmite was present as fibres or needles that were up to 200 nm long in sample A(a), as shown in Fig. 6a, and that were up to 50 nm long in sample AZ(a), as shown in Fig. 6b. The material with the short needles was much easier to peptize than that containing the 200 nm fibrillar crystals. After calcination at 800 °C, all samples, whether autoclaved or not, looked rather similar and consisted of equiaxed crystals approximately 3–5 nm in diameter, as shown in Fig. 7. The TEM estimate of crystallite size was in good agreement with average γ-Al_2O_3 crystallite size calculated from XRD peak broadening.

TABLE I Phase composition and crystallite size of various alumina samples as determined by XRD

Sample designation	Phase composition and lattice parameters (nm)				Crystallite size (nm)[a, b]				Lattice strain (%)		
	600 °C	800 °C	1000 °C	1200 °C	600 °C	800 °C	1000 °C	1200 °C	600 °C	800 °C	1000 °C
A	Amorphous	γ a = ND	γ a = 0.7901	α a = 0.4762 c = 1.3001	– (8)	ND (10)	10 (15)	100	–	–	0.842
AZ	Amorphous	γ a = ND	γ a = 0.7903	α + θ a = 0.4763 c = 1.3002	– (6)	ND (10)	9 (15)	50	–	–	0.904
A(a)	γ a = 0.7917	γ a = 0.7916	γ a = 0.7912	α a = 0.4762 c = 1.3001	5 (6)	6 (7)	9 (14)	80	1.411	1.283	0.930
AZ(a)	γ a = 0.7919	γ a = 0.7911	γ a = 0.7911	θ a = 1.1807 b = 0.2917 c = 0.5627 β = 104.12°	4 (5)	5 (8)	9 (16)	60	1.781	1.47	0.908

[a] Calculated from the Scherrer equation.
[b] Values in brackets calculated from $D = 6/\rho S$, where D is the average particle size, ρ is the density (Al_2O_3 = 3.98 g cm^{-3}) and S is the specific surface area.
[c] ND not determined.

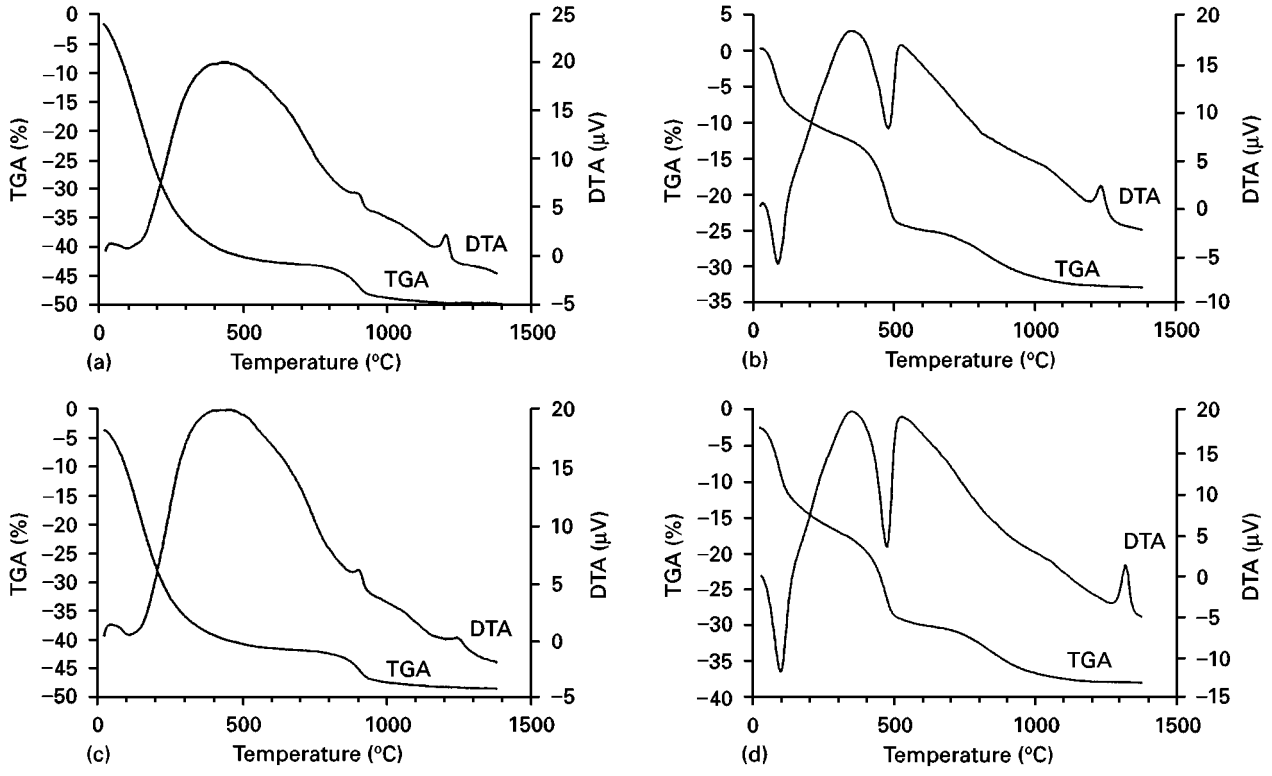

Figure 4 Thermogravimetric and differential thermal analysis of various alumina samples: (a) sample A–Al_2O_3, (b) sample A(a)–Al_2O_3 autoclave treated, (c) sample AZ–Zr-doped Al_2O_3 (d) sample AZ(a)–Zr-doped Al_2O_3 autoclave treated.

After calcination at 1000 °C, the samples A and AZ consisted of well crystallized γ-Al_2O_3. The samples A(a) and AZ(a) were generally similar, but some δ-Al_2O_3 was also present. The spherical aggregate shape in samples A and AZ remained largely unchanged as shown in Fig. 8, although sample AZ also contained a small amount of sheet-like aggregate that was probably produced during the drying of the precipitate. The morphology in the mixed γ- and δ-Al_2O_3 phases in samples A(a) and AZ(a) was not uniform; there were areas similar to the γ-Al_2O_3 structure of samples A and AZ as shown in Fig. 8, but there were also areas exhibiting some kind of ordering in dendritic clusters as shown in Fig. 9.

The morphology of the samples after calcination at 1200 °C was significantly different. In sample A each spherical aggregate appeared to be a single crystal of α-Al_2O_3 as shown in Fig. 10a; although in dark field

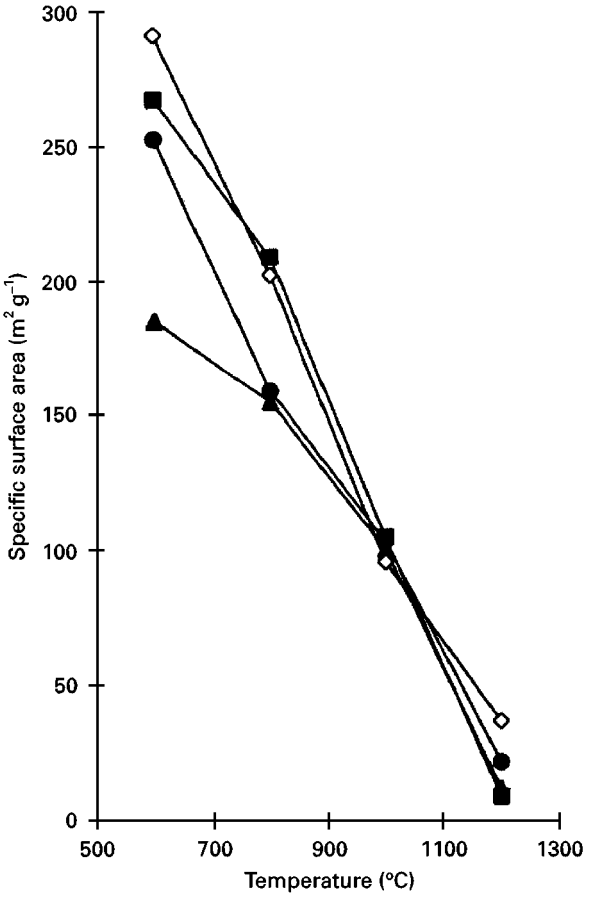

Figure 5 The dependence on temperature of specific surface area for various alumina samples. (▲) A, (■) A(a), (●) AZ, (◇) AZ(a).

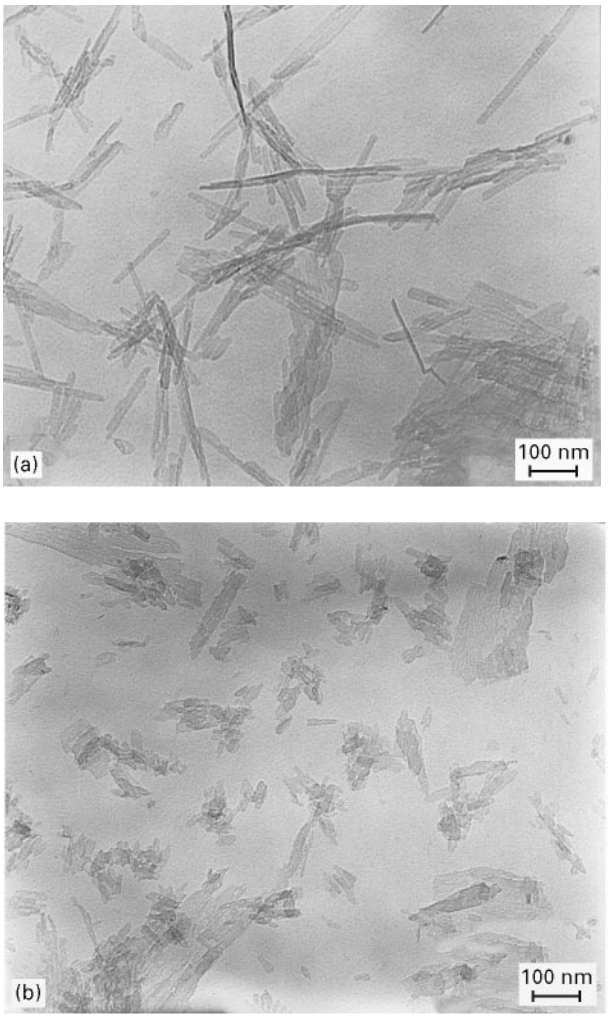

Figure 6 TEM micrographs showing the morphology of boehmite crystals in pure and Zr-doped autoclave treated materials: (a) sample A(a), and (b) sample AZ(a).

TEM, e.g. Fig. 10b, these single crystals exhibit variations in contrast. This type of structure has been observed previously [21], and was attributed to single-crystals with sufficient variation in Bragg diffraction angle to effect contrast changes as indicated in Fig. 10c. Strains associated with the removal of porosity and process of crystal growth within the spherical agglomerate structure may be the cause of this anomaly. After longer calcination times, α-Al_2O_3 crystals grow in a characteristic finger-like morphology as shown in Fig. 10d. A mechanism for the growth of finger-like crystals in alumina has been proposed [5]. The morphology of the autoclave treated alumina sample A(a) after calcination at 1200 °C for 1 h is very similar to that shown in Fig. 10d. The AZ sample, however, contained two characteristic morphologies: first, there were finger-like α-Al_2O_3 crystals, which are smaller in size than in the pure alumina samples, i.e. samples A and A(a), and second, there were agglomerates that still contained a small amount of θ-Al_2O_3 together with small α-Al_2O_3 crystals. In contrast, the AZ(a) sample contained only θ-Al_2O_3 agglomerates, as shown in Fig. 11, with a crystallite size of about 60 nm.

After calcination at 1200 °C for 100 h, the pure alumina samples, A and A(a), consisted of large crystals of α-Al_2O_3 with some closed porosity. The Zr-doped alumina samples, AZ and AZ(a), consisted of porous nanocomposite agglomerates comprising zirconia particles of up to 50 nm diameter distributed within α-Al_2O_3 crystals and decorating the edges of pores as shown in Fig. 12.

4. Discussion

The effects of the ZrO_2 dopant and of the autoclave treatment on the chemical composition, microtexture and phase composition of the calcined product are summarized in Table I. These results showed that the structural characteristics of the transition aluminas, whether pure alumina or zirconia-doped alumina, depended strongly on their thermal history during dehydration and calcination. Autoclave treatment yielded well crystallized dehydration products: either fibrillar boehmite in the case of pure alumina, or acicular boehmite in the case of Zr-doped alumina and formed at less than 600 °C. In contrast, calcination in air yielded much less well ordered structures with both the pure and the Zr-doped alumina remaining essentially amorphous up to about 800 °C.

Both the autoclave treatment and the use of Zr dopant appeared to increase the temperature of the transformation to α-Al_2O_3 compared with that of the air-calcined pure alumina. However, because the transition phases are metastable phases, the increases

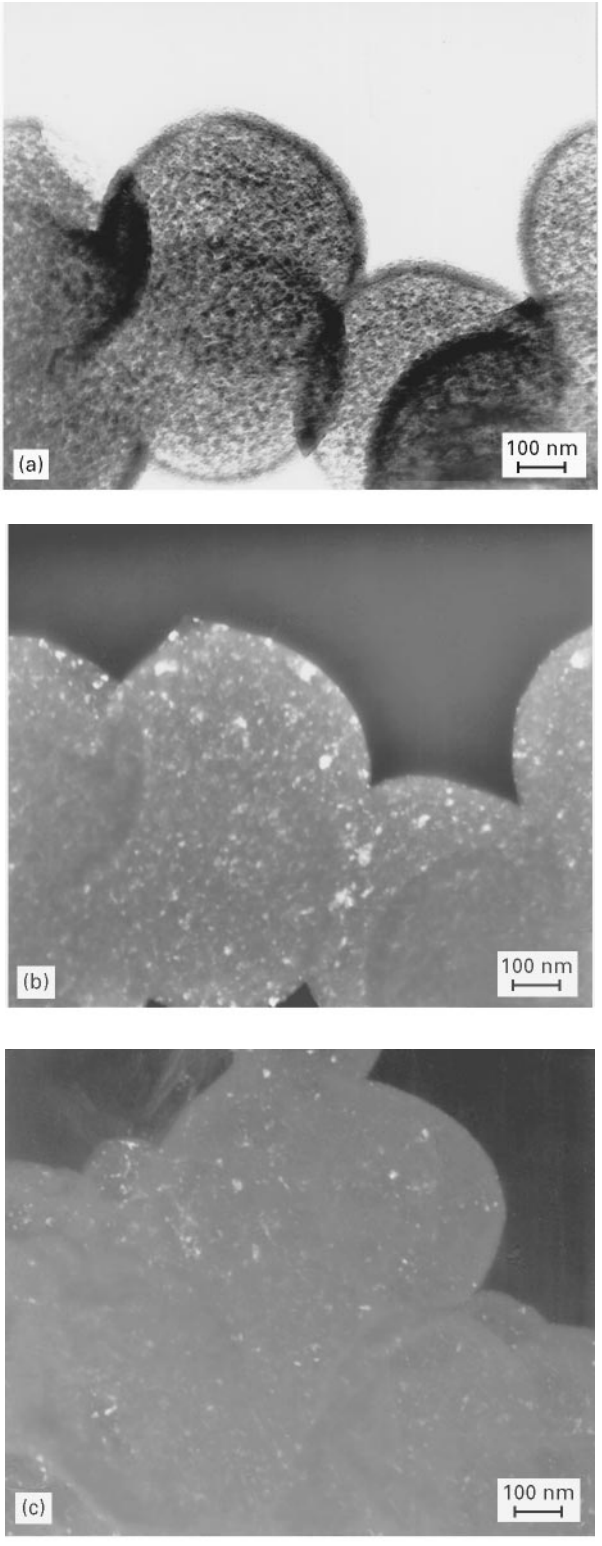

Figure 7 TEM micrographs showing particle morphology after calcination at 800 °C for 1 h: (a) bright field image of sample A, (b) dark field image of same sample, and (c) dark field image of sample AZ.

in transformation temperatures indicated by DTA are more correctly interpreted as being indicative of slower kinetics of transformation to α-Al_2O_3. For example, whereas after 1 h at 1200 °C only the AZ(a) material had not transformed to α-Al_2O_3, the transformation to α-Al_2O_3 did occur at 1200 °C in this material after 100 h. However, at 1100 °C the transformation kinetics in the same material would be so slow that for all practical purposes it is convenient to regard the material as stable at that temperature. We therefore refer to the delayed transformation as an increased thermal stability of the transition phases. There would seem to be two ways in which the thermal stability is increased. The autoclave treatment increases stability through improving crystal perfection, whereas Zr enters the lattice and modifies the lattice energy. We can

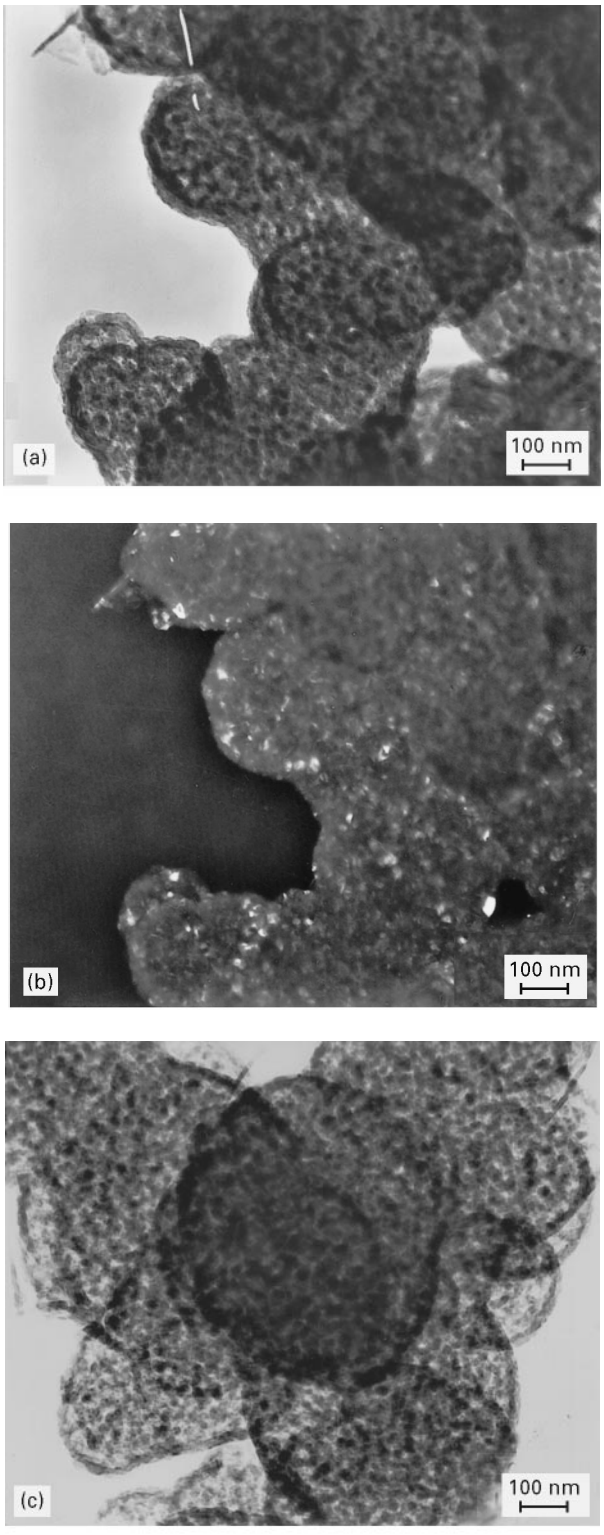

Figure 8 TEM micrographs showing particle morphology after calcination at 1000 °C for 1 h: (a) bright field image of sample A, (b) dark field image of same sample, (c) bright field image of sample AZ, and (d) dark field image of sample AZ.

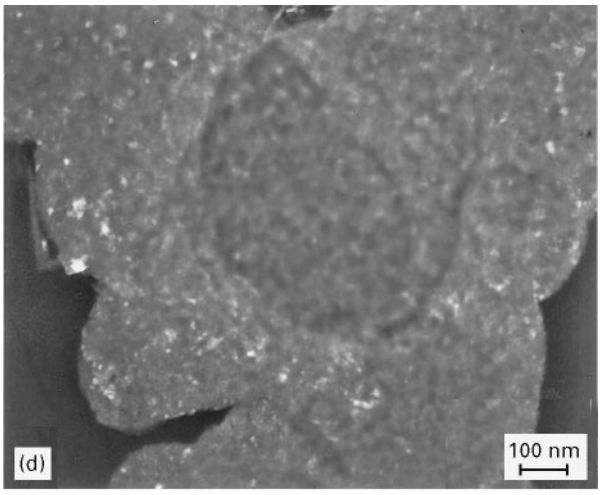

Figure 8 (Continued)

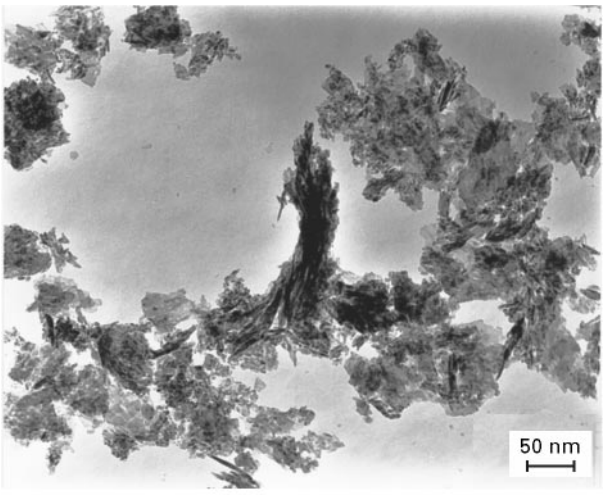

Figure 9 TEM micrograph showing the heterogeneous morphology in Zr-doped alumina, sample AZ(a), calcined at 1000 °C for 1 h.

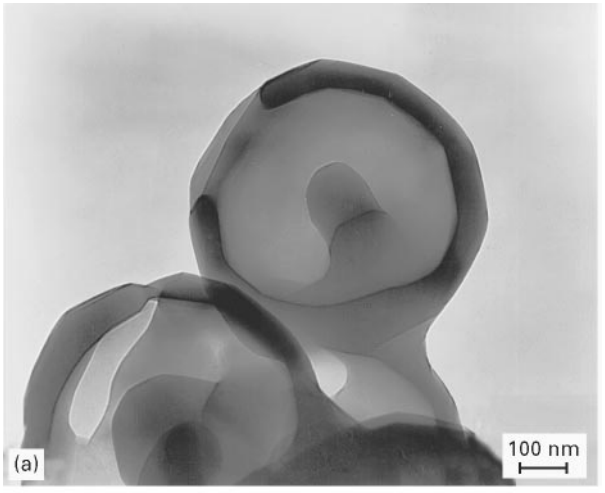

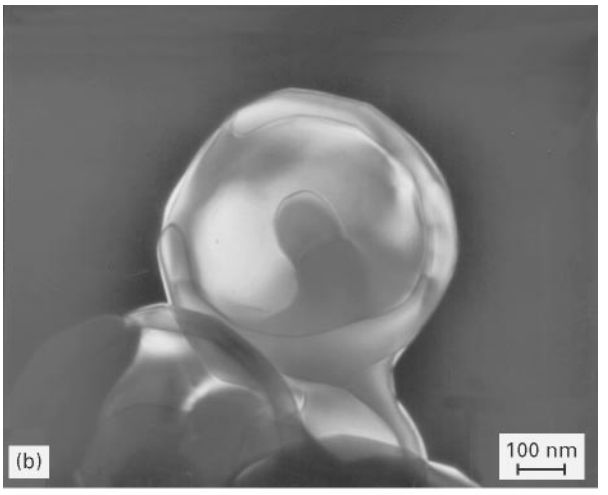

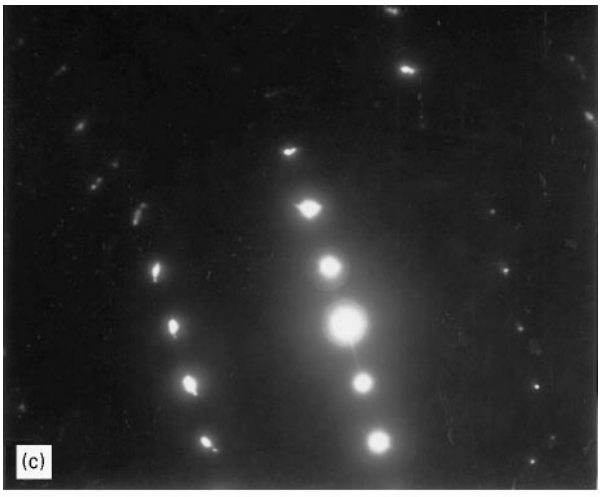

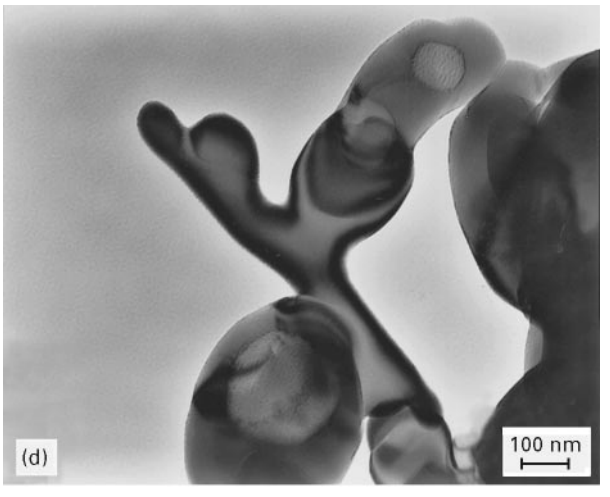

Figure 10 TEM micrographs (a, b, d) and diffraction pattern (c) showing single crystals of α-Al_2O_3 calcined at 1200 °C for 30 min: (a) bright field image of sample A, (b) dark field image of sample A, (c) diffraction pattern from sample A, (d) bright field image of finger-like morphology sample AZ after 1 h at 1200 °C.

deduce that the Zr dopant dissolved in the alumina, thereby entering the lattice, from the failure to detect any separate zirconia phase (cubic, tetragonal or monoclinic) for calcination temperatures below 1200 °C. Dissolution of Zr in the alumina lattice implies the presence of Al–O–Zr bonding and it is to these bonds that we attribute the contribution of Zr to the stabilization of the transition structures in Zr-doped material. The autoclave treatment promotes well crystallized structures that are energetically more stable than poorly crystallized material of the same composition. In the Zr-doped alumina the transformation of the

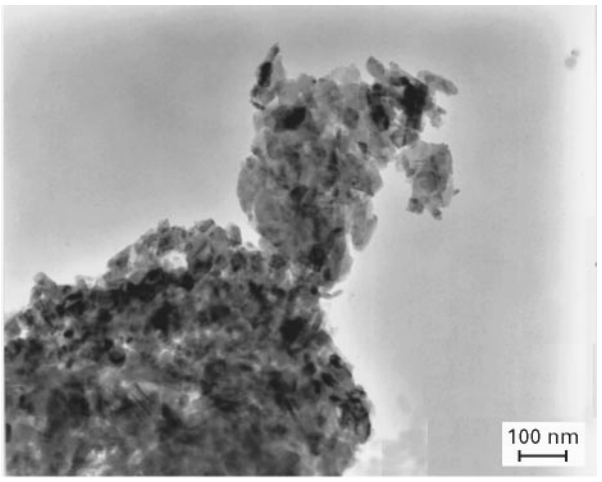

Figure 11 Bright field TEM micrograph showing agglomerates of θ-Al_2O_3 in sample AZ(a) calcined for 1 h at 1200 °C.

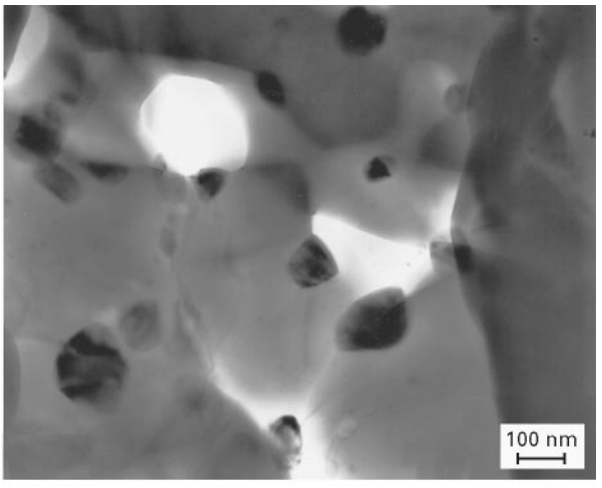

Figure 12 Bright field TEM micrograph of Zr-doped alumina, sample AZ(a), calcined for 100 h at 1200 °C showing a nanocomposite structure with t-ZrO_2 particles distributed predominantly at pore surfaces.

θ-phase into α-Al_2O_3 is associated with a partitioning of phases (t-ZrO_2 and α-Al_2O_3), which is an energetically more difficult process to nucleate than simple recrystallization due to creation of a large specific interface area associated between the very fine particles of t-ZrO_2 (less than 50 nm) and the surrounding α-Al_2O_3 grains as shown by TEM and XRD results. This partitioning of phases leads to the formation of an Al_2O_3–ZrO_2 nanocomposite as shown in Fig. 12.

We believe that Al–O–Zr bridges are formed during the dehydration and dehydroxylation of Zr-doped alumina while the structure is relatively amorphous. On crystallization of the structure, however, the degree of solid solubility of Zr in transition alumina and in α-Al_2O_3 will depend on the availability of suitable cation sites in these phases. In the α-Al_2O_3 structure, each Al^{3+} is co-ordinated by six oxygen ions, whereas in the metastable aluminas, which have a spinel structure, Al^{3+} is distributed among sites co-ordinated by either four or six oxygen ions. For example, the spinel structure of γ-Al_2O_3 has a unit cell with 24 cation sites and 32 anion sites. The oxygen ions in the anion sites form a c.c.p. lattice and, to maintain stoichiometry, the aluminium ions occupying only $21\frac{1}{3}$ sites of the 24 available sites. Therefore, although the ionic radius of Zr^{4+} is too large to permit direct substitution for Al^{3+} in either the octahedral or tetrahedral sites, the mixture of two types of cation sites, and the presence of vacant sites, facilitates an adjustment in the distribution of the Al^{3+} cations to allow the accommodation of Zr^{4+} in the transition alumina lattices. However, this freedom of structural arrangement in the spinel lattices of the transitional aluminas does not exist in the α-Al_2O_3 lattice. In consequence, because the α-Al_2O_3 lattice cannot provide sites to accommodate Zr^{4+}, the transformation from the transition phase to α-Al_2O_3 must be accompanied by a phase partition.

The proposed existence of an essentially amorphous polymer-like structure with Al–O–Zr bridges, and the observations made concerning the subsequent crystallization and phase evolution, are consistent with a number of other reported results, i.e. those of Balmer *et al.* [22] on metastable solid solutions of composition $Zr_{1-x}Al_xO_{(2-x/2)}$, the results of Yamaguchi *et al.* [23] on cubic ZrO_2 solid solutions in the Al_2O_3–ZrO_2 system, and with results of Pugar and Morgan [24] on copolymerized alkoxide network with an Al–O–Zr structure. It is possible that the incorporation of Zr^{4+} into the lattice of transition alumina is also made easier by the fact that some of the Al^{3+} cations may initially be located in non-optimum sites within the lattice. For example, the dehydration of boehmite leaves Al^{3+} ions in non-optimum sites in γ-Al_2O_3, leading to lattice distortion, which is relieved by rearrangement at higher temperatures. The exact nature of this lattice distortion is not yet fully clarified, however, and a number of possible structures have been proposed, for example, a spinel structure with tetragonal distortion [20], a tetragonal unit cell with a slightly shortened *c*-axis [3], a tetragonal structure with $a = 0.796$ nm and $c = 0.781$ nm, and a cubic structure with $a = 0.790$ nm [6]. If we assume that the structure of the alumina is cubic, our lattice parameters (Table I) are in good agreement with reported values.

Whereas it is plausible to argue that Zr solubility in transition alumina derives from the ability of Al^{3+} to occupy a variety of cation sites, it cannot be argued that Zr^{4+} dopant plays any role in determining the distribution of Al^{3+} ions among those sites. Lattice parameter measurements clearly indicate that only the synthesis conditions, i.e. autoclave treatment or air-calcination, and not the presence of the Zr dopant, determine the lattice structure. A difference in the dehydroxylation mechanism operating in material subjected to autoclave treatment compared with that in material calcined in air would be consistent with this observation. For autoclaved materials, the decrease of about 0.1% in the *a*-parameter and a reduction of about 0.4% in lattice strain values suggested that there was a slight increase in lattice ordering after calcination at 1000 °C compared with calcination at 800 °C. Unfortunately, the air-calcined material was not sufficiently well crystallized after calcination at 800 °C to enable a similar comparison for the non-

autoclaved material to be made. However, after calcination at 1000 °C for 1 h, all samples were well crystallized, and the *a*-parameter in the autoclaved materials, i.e. samples A(a) and AZ(a), was found to be significantly larger than that for air-calcined samples, i.e. samples A and AZ. We attribute this difference in lattice parameter to a difference in Al^{3+} ordering, which in turn originates from differences in the dehydroxylation mechanism in the precursor phase.

The XRD results for the A(a) and AZ(a) samples calcined at 1000 °C for 1 h indicated a doubling of the 400 and 440 peaks, which is consistent with the reported d-values of alumina [4-877JCPDS-ICDD], and which we therefore ascribed to the presence of δ-Al_2O_3 in these samples. The presence of δ-Al_2O_3 has also been reported in alumina produced by the Aerosil-method (aluminium oxide) [25] and in alumina produced from boehmite [20]. In contrast, we found no evidence for δ-Al_2O_3 in the A and AZ samples calcined at the same temperature. Thus, although the transition aluminas that we found in our samples included γ-Al_2O_3, δ-Al_2O_3 and θ-Al_2O_3, the δ-phase was only observed as a minor constituent in the autoclaved samples A(a) and AZ(a) at one calcination temperature only. Whereas the γ-Al_2O_3 phase still contains hydroxyl species, the δ-Al_2O_3 and θ-Al_2O_3 phases are nearly dehydroxylated and the degree of ordering in the structure increases in the series: $\gamma \rightarrow \delta \rightarrow \theta$. However, the transformation from the γ- to the θ-phase is associated not only with dehydroxylation but also with improved ordering of Al^{3+} ions in the lattice.

In contrast to the transformations between different forms of transition alumina, the transformation of θ- to α-Al_2O_3 involves a much greater structural rearrangement. Nevertheless, the mechanism is still not completely clear and two different types of mechanism have been suggested. The mechanism that seems most consistent with our results is a conventional nucleation and growth process [5, 21, 26–28] that initiates at a site of low activation energy, such as a site on the particle surface, or at a neck between particles. The effect of dopant on such a mechanism would be to block the most reactive sites for nucleation of the α-phase as suggested by Oudet *et al.* [29] to explain the stabilization of transition aluminas by La-dopant.

The size and morphology of α-Al_2O_3 crystals, particularly in the early step of crystal growth at 1200 °C, seemed to depend on the characteristics of the uncalcined precursor: the crystals of Zr-doped samples were smaller and with a more pronounced finger-like morphology than those of undoped samples. This finding contrasts with that for samples calcined at 1000 °C for 1 h for which crystallite size in all samples was very similar at about 9–10 nm so that, for this calcination temperature, there was no evidence to suggest that the ZrO_2 dopant or the autoclave treatment had any effect on crystallite size or shape. The characteristic appearance of α-Al_2O_3 crystals that developed within spherical aggregates at 1200 °C is shown in Fig. 10a and b. The dark-field contrast shows variations in brightness within spheres that might normally be taken to indicate that the spheres were polycrystalline; however, the electron diffraction pattern indicates that each sphere is a single crystal. This apparent anomaly is believed to result from regions of lattice distortion within each crystal that cause local deviations in the Bragg diffraction angle sufficient to appear as brightness variations in TEM dark-field images as reported earlier by Tucker [21]. It seems unlikely that this phenomenon was a direct result of the growth of the α-Al_2O_3 crystals, which would occur by the diffusion of atoms and vacancies at the moving crystal interface and which would result only in the elimination of porosity and in the shrinkage of spheres. This is a process that would tend to relieve stress rather than to generate it. The fact that each sphere develops into a single crystal is consistent with the earlier suggestion that the α-Al_2O_3 phase nucleation occurs preferentially at the neck between two spheres [21] and is followed by growth. However, the development of facets on the spheres points to the presence of additional mechanisms, such as the filling of oxygen vacancies preferentially at the surface of spheres that might plausibly explain how both facets developed on the crystals and also how local strains were induced, to the extent that the spheres distorted to produce slight deviations in the Bragg angle across the crystal.

An alternative mechanism that has been proposed for the θ- to α-Al_2O_3 transformation should also be mentioned. This is diffusion controlled growth of the θ-Al_2O_3 crystallites to a critical size followed by synchro-shear martensitic type transformation of θ- to α-Al_2O_3 [26]. In the AZ(a) sample calcined at 1200 °C for 1 h, the well defined θ-phase has a crystallite size of 60 nm (calculated from XRD peak broadening), which is similar to the critical size reported by Wynnyckyj and Morris [26] on the basis of XRD measurements corresponding to 20–40 nm as measured by TEM. The postulated diffusionless, co-operative transformation (the diffusionless rearrangement of both oxygen and aluminium sublattices) might be expected to be inhibited by the presence of a dopant and such a mechanism would therefore be consistent with the observed delayed transformation from θ- to α-Al_2O_3 in the AZ(a) sample. The difference in behaviour between AZ and AZ(a) seems less likely to be due to any differences in the distribution of Al–O–Zr bonding in the gel-like solids formed by autoclave treatment than to the different distribution of Al^{3+} ions in the lattice in autoclaved materials as reflected in the larger lattice parameter as discussed earlier. However, although a mechanism based on a martensitic type transformation is consistent with a number of our observations, it seems quite unable to account for the existence of the large single crystal particles of α-Al_2O_3 that we observed, and hence we do not consider the martensitic transformation to be the θ- to α-Al_2O_3 transformation mechanism operating in our materials.

The various possible mechanisms discussed above indicate that several factors may influence the transformation of transition phases to α-Al_2O_3 and that the process is complex. We believe that nature of the dopant (valency and ionic radius) affected the nucleation and growth of the α-phase through the creation of

additional point defects and through the interaction of point defects in alumina with those in zirconia. The filling of oxygen vacancies in zirconia and alumina is a competitive process. The γ-phase has a tetragonal distorted lattice that was described by Burtin *et al.* [13] as

$$Al_2\square O_{3-v/2}(OH)_v\langle\rangle_{1-v/2}$$

where: $\square$ = a cation vacancy and $\langle\rangle$ = an oxygen vacancy. For $v = 0$, the formula is $Al_2\square O_3$, which corresponds to α-Al_2O_3 in which one-third of the octahedral cation sites are unoccupied. For $v = 2$, the formula is $Al_2\square O_2(OH)_2$, which corresponds to boehmite [2AlO(OH)]. The effect of Zr^{4+} on cation vacancies (number and distribution), and particularly on oxygen vacancies is believed to be significant, particularly if the Zr dopant is incorporated into the lattice structure through Al–O–Zr bridging as in sample AZ(a). The tetrahedral sites in the lattice of the γ-phase are larger than the octahedral sites, but the ionic radius of Zr^{4+} (0.079 nm) is larger than that of Al^{3+} (0.051 nm) and is too large to fill interstitial positions. Boehmite has only octahedral co-ordination, so that octahedral interstices could be occupied in the resulting γ-Al_2O_3 at lower temperatures (about 600 °C). The lattice parameter $a = 0.7919$ nm after calcination at 600 °C compared with $a = 0.7911$ nm after calcination at 1000 °C in the AZ(a) samples indicated an increase in ordering in the γ-phase with an increase in calcination temperature. The tendency to non-stoichiometry or oxygen vacancies in zirconia [30] could create competitive cation–oxygen ordering leading eventually to phase partitioning and the nucleation of the α-Al_2O_3. Both TEM and XRD examinations in our Zr-doped samples confirmed that the transformation to the α-phase was accompanied by a partitioning of phases. This is consistent with other results reported for phase partitioning in the Al_2O_3–ZrO_2 system [22–24], and a phase partition mechanism based on the annihilation of anionic and cationic vacancies has been proposed by Burtin *et al.* [13].

After calcination at 1200 °C for 1 h, the autoclave treated Zr-doped sample consisted entirely of θ-phase and had a specific surface area of 36 $m^2 g^{-1}$. The presence of the zirconia dissolved in transition phases therefore certainly stabilized the transition phase and it is also expected to alter the surface chemistry properties with respect to pure alumina. For example, it is reported [31] that the incorporation of zirconia into the washcoat of car catalysts improves thermal stability and reduces the dissolution of the rhodium into the washcoat. Furthermore, the presence of sulfate anions, retained from the zirconium sulfate precursor, can increase the acidity, i.e. increase the concentration of acidic sites, for catalytic applications [31]. The level of sulfate anion impurities in precipitates can be controlled through the amount of washing to which the precipitate is subjected. The fine distribution of the zirconia dopant and its ability to accommodate a deficiency in oxygen [30, 32] could be important for design of the catalytic properties of this material, especially for the reduction of gases such as NO at surfaces and their interaction with CO.

5. Conclusions

Spherical particles of pure and Zr-doped hydrated basic aluminium sulfate were precipitated from acidified solution by the thermal decomposition of urea. Autoclave treatment of this amorphous precipitate at 210 °C yielded acicular or fibrillar nanocrystals of the monohydrate, boehmite. Weight losses from the non-autoclave treated precipitates during calcination in air were consistent with a composition corresponding to a trihydrate. The non-autoclaved material remained amorphous up to about 800 °C before transforming to γ-Al_2O_3. The autoclave treated precipitate, however, transformed to γ-Al_2O_3 at the significantly lower temperature of about 600 °C, and also yielded a higher specific surface area. The lattice parameters of γ-Al_2O_3 from boehmite were significantly larger (0.1%) than for γ-Al_2O_3 from the amorphous trihydrate, even after lattice strain had been relieved to the same levels in both materials. The γ-Al_2O_3 from boehmite was also more stable with respect to transformation to α-Al_2O_3. It is assumed that these differences between the two materials are attributable to differences in the distribution of aluminium cations resulting from dehydroxylation processes. The greatest degree of stability in transition alumina was obtained using the combination of Zr dopant and autoclave treatment and resulted in the retention of θ-Al_2O_3 after 1 h at 1200 °C and a specific surface area of 36 $m^2 g^{-1}$. In Zr-doped material, transformation to α-Al_2O_3 occurred by phase partitioning with the formation of an Al_2O_3–ZrO_2 nanocomposite. We conclude that the morphology of transition phase aluminas is modified both by the autoclave treatment to crystallize boehmite and also by the addition of Zr dopant, and that these structural modifications significantly increase the thermal stability of the transition phases.

Acknowledgements

The authors gratefully acknowledge contributions from Dr. R. de Jong in discussions of this work, from Mr. R. G. Nyqvist in making the BET surface area measurements, and from Dr. I. J. Davis for some of the TEM pictures.

References

1. H. C. STUMPF, A. S. RUSSELL, J. W. NEWSOME and C. M. TUCKER, *Ind. Engng. Chem.* **42** (1950) 1398.
2. G. ERVIN, Jr, *Acta Crystallogr.* **5** (1952) 103.
3. H. SAALFELD, *Clay Min. Bull.* **3** (1985) 249.
4. A. J. LEONARD, F. VAN CAUWELAERT and J. J. FRIPIAT, *J. Phys. Chem.* **71** (1967) 695.
5. P. A. BADKAR and J. E. BAILEY, *J. Mater. Sci.* **11** (1976) 1794.
6. S. J. WILSON, *Proc. Brit. Ceram. Soc.* **28** (1979) 281.
7. S. J. WILSON and J. D. C. McCONNELL, *J. Solid State Chem.* **34** (1980) 315.
8. H. S. SANTOS, P. K. KIYOHARA and P. S. SANTOS, *Ceram. Int.* **20** (1994) 175.
9. T. FUKUI and M. HORI, *J. Mater. Sci. Lett.* **13** (1994) 413.
10. A. UENO, in Proceeding of the 11th Symposium on Catalytic Combustion, Tokyo, May 1991, (1991) p. 1–8.
11. Y. MIZUSHIMA and M. HORI, in Proceedings of the Eurogel '91 Conference, edited by S. Vilminot, R. Nass and H. Schmidt, Saarbrucken, Germany, 1991 (Elsevier, Amsterdam, 1992) p. 195–201.

12. P. BURTIN, J. P. BRUNELLE, M. PIJOLAT and M. SOUSTELLE, *Appl. Catal.* **34** (1987) 225.
13. *Idem*, *ibid.* **34** (1987) 239.
14. R. K. ILER, *J. Amer. Ceram. Soc.* **47** (1964) 339.
15. B. BEGUIN, M. E. GARBOWSKI and M. PRIMET, *J. Catal.* **127** (1991) 595.
16. M. MACHIDA, K. EGUCHI and H. ARAI, *ibid.* **103** (1987) 385.
17. G. GROPPI, C. CRISTIANI, P. FORZATTI and M. BELLOTTO, *J. Mater. Sci.* **29** (1994) 3441.
18. R. BRACE and E. MATIJEVIC, *J. Inorg. Nucl. Chem.* **35** (1973) 3691.
19. M. D. SACKS, T.-Y. TSENG and S. Y. LEE, *Ceram. Bull.* **63** (1984) 301.
20. B. C. LIPPENS and J. H. DE BOER, *Acta Crystallogr.* **17** (1964) 1312.
21. D. S. TUCKER, *J. Amer. Ceram. Soc.* **68** (1985) C163.
22. M. L. BALMER, F. F. LANGE and G. C. LEVI, *ibid.* **77** (1994) 2069.
23. O. YAMAGUCHI, M. SHIRAI and M. YOSHINAKA, *ibid.* **71** (1988) C510.
24. E. A. PUGAR and E. D. MORGAN, *ibid.* **69** (1986) C120.
25. M. R. GALLAS and G. P. PIERMARINI, *ibid.* **77** (1994) 2917.
26. J. R. WYNNYCKYJ and C. G. MORRIS, *Metall. Trans. B* **16** (1985) 345.
27. D. S. TUCKER, E. J. JENKINS and J. J. HREN, *J. Electron Microsc. Technol.* **2** (1985) 29.
28. F. W. DYNYS and J. W. HALLORAN, *J. Amer. Ceram. Soc.* **65** (1982) 442.
29. F. OUDET, P. COURTINE and A. VEJUX, *J. Catal.* **114** (1988) 112.
30. B. DJURIČIČ, S. PICKERING, D. McGARRY, P. GLAUDE, P. TAMBUYSER and K. SCHUSTER, *Ceram. Int.* **21** (1995) 195.
31. F. R. CHEN, G. COUDURIER, J. F. JOLY and J. C. VEDRIN, *J. Catalysis* **143** (1993) 616.
32. J. LIVAGE, K. DOI and C. MAZIERES, *J. Amer. Ceram. Soc.* **51** (1968) 349.

Received 23 February
and accepted 17 July 1996